PROCEEDINGS OF SPIE

SPIEDigitalLibrary.org/conference-proceedings-of-spie

Lens mounting techniques for precise radial location of fragile lenses in the NGS2 and Veloce instruments

Nicholas Herrald, Francis Bennet, Celine D'Orgeville, Francois Rigaut, Ian Price, et al.

Nicholas Herrald, Francis Bennet, Celine D'Orgeville, Francois Rigaut, Ian Price, James Gilbert, "Lens mounting techniques for precise radial location of fragile lenses in the NGS2 and Veloce instruments," Proc. SPIE 10706, Advances in Optical and Mechanical Technologies for Telescopes and Instrumentation III, 107064C (10 July 2018); doi: 10.1117/12.2311895

SPIE.

Event: SPIE Astronomical Telescopes + Instrumentation, 2018, Austin, Texas, United States

Lens mounting techniques for precise radial location of fragile lenses in the NGS2 and Veloce instruments

Nicholas Herrald[a], Francis Bennet[a], Celine D'Orgeville[a], Francois Rigault[a], Ian Price[a], and James Gilbert[a]

[a]Research School of Astronomy and Astrophysics, The Australian National University, Advanced Instrumentation and Technology Centre, Canberra, Australia

ABSTRACT

We present novel methods for mounting lenses in a pair of instruments that presented challenging optical and mechanical requirements. The first instrument is the replacement Natural Guide Star Sensor (NGS2) for CANOPUS at Gemini South, which incorporates an objective consisting of a stack of six lenses mounted in a common bore. A compliant radial spacer was used to eliminate lens decentre resulting from the additional radial clearance required to accommodate differential thermal strains between the low thermal expansion lenses and a common bore. In the same instrument, tangent contact toroidal spacers were deployed in place of traditional conical spacers to further reduce contact stresses in fragile calcium fluoride lens elements. The toroidal faces were specified with a $10\mu m$ profile tolerance to avoid possible edge contact between the spacers and lenses. We investigated milling and turning machining processes for the production of the spacers by comparing their results via Coordinate Measuring Machine (CMM) measurements. In the second instrument, Veloce, built for the Anglo-Australian Telescope, a lens decentre requirement of $40\mu m$ led us to develop a simple means of in-situ centring adjustment of the cell mounted lens. Physical testing of the finished instruments verified the performance of each of these methods. NGS2 produced images at the factory acceptance test in which 94% of encircled energy was captured by a single 16um detector pixel, surpassing the specification of 80%. Bench testing of Veloce during assembly showed that the adjustment mechanism allowed centring of the lens over a range of +/- 0.1mm with a precision of $5\mu m$.

Keywords: optomechanics, lens centring, toroidal lens seat, fragile lenses, NGS2, Veloce, ANU

1. NGS2 OVERVIEW

NGS2 is a multi-natural guide star sensor, used for tip-tilt and plate scale mode sensing in the Canopus instrument at Gemini South. The sensor was built between 2014 and 2016 by the Australian National University. It has undergone factory acceptance testing at ANU in 2016 and is currently awaiting installation and commissioning at Gemini South. The optical layout of the sensor re-images the f16 wave-front sensor input beam to f1.80 at the detector, which is a single NuVu EM-CCD array. The optical modules in the sensor consist of a pair of periscope alignment mirrors, the "Tube Lens" assembly consisting of a pair of lenses, a third adjustable fold mirror and the "Objective" assembly, consisting of a stack of six lenses.

The six lenses of the Objective Assembly (including one doublet) are mounted within a common housing. Five of the six lenses are mounted within a single bore in the housing, with the sixth mounted in a smaller concentric bore. The pre-load force maintaining contact between the lenses are their seats is provided by a wave spring which is loaded against the lens and spacer stack by the outer cap of the housing. A cross-section view of the objective assembly is shown in Figure 1.

Further author information: (Send correspondence to Nicholas Herrald)
Nicholas Herrald: E-mail: nick.herrald@anu.edu.au, Telephone: 61 2 6125 0205

Advances in Optical and Mechanical Technologies for Telescopes and Instrumentation III, edited by Ramón Navarro, Roland Geyl, Proc. of SPIE Vol. 10706, 107064C · © 2018 SPIE
CCC code: 0277-786X/18/$18 · doi: 10.1117/12.2311895

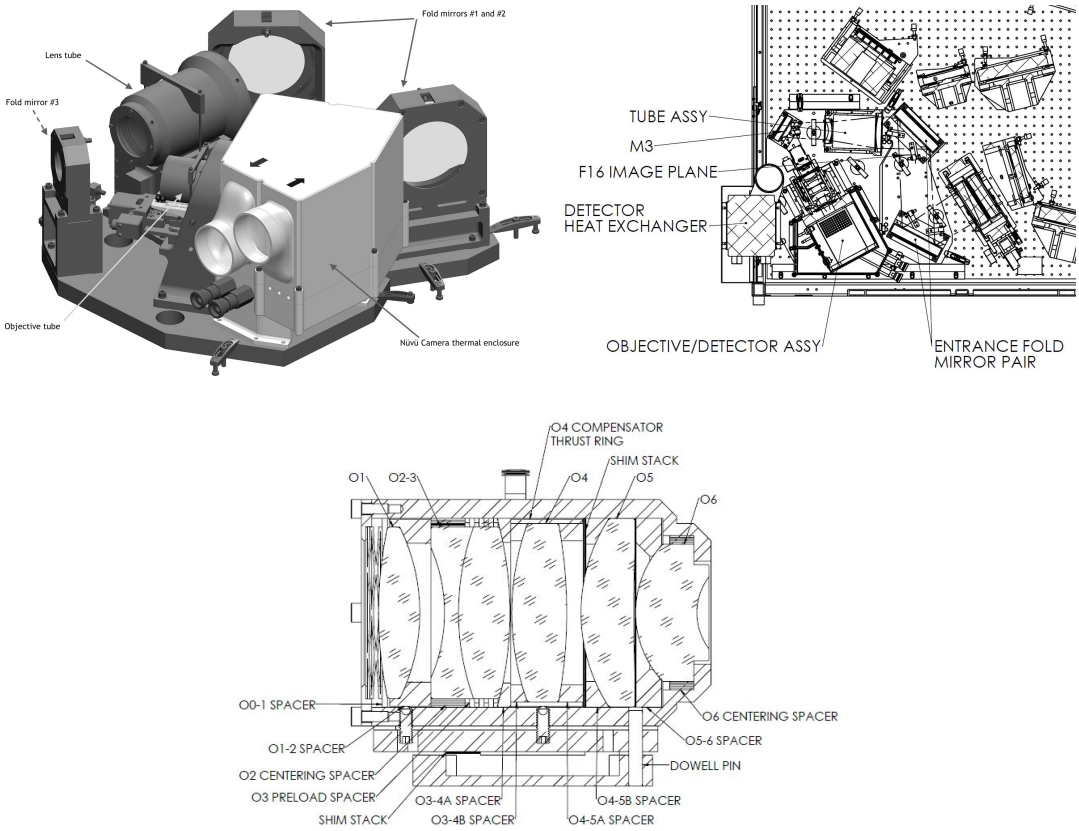

Figure 1. NGS2 Instrument isometric view (left), NGS2 in position on Canopus optical bench (right) and cross section view of Objective Assembly (bottom).

2. OBJECTIVE ASSEMBLY DESIGN CHALLENGES

The challenges of mounting the lenses within the NGS2 Objective Assembly stem primarily from the fact that several of the lenses are made from Calcium Fluoride, which has both a high coefficient of thermal expansion (COTE) and a high susceptibility brittle fracture compared to the glasses of the other lenses. The high thermal expansion of CaF2 relative to the other glasses in the Objective Assembly led the design team to opt for a novel decentre control method (described in Sec. 2.6). The fragility of these lenses, combined with a high pre-load requirement for the objective assembly, led the design team to develop the novel form of the lens spacers contacting CaF2 lenses (described in Sec. 2.1).

2.1 Contact stresses in CaF_2 lenses

Seating surfaces within a lens mounting bore which form a line contact with spherical lens surfaces are a well established means of providing accurate axial location of spherical lenses. Contact stresses in lenses at the interface between the metal seats and the glass of the lenses depends on the respective radii of both surfaces and on the stiffness of the lens and seat material. Hertzian contact mechanics gives the compressive contact stress (σ_c) at the lens/seat interface for a general case of contact between a spherical lens and its seat as

$$\sigma_C = 0.798 \left(\frac{K_1 p_i}{K_2} \right)^{\frac{1}{2}} . \quad (1)$$

The constants, K_1 and K_2 respectively represent combined geometrical and material moduli of the two sides of the interface, and p_i is the load per unit length of the line contact. These moduli are given by

$$K_1 = \frac{R_1 \pm R_2}{2(R_1 R_2)}, \tag{2}$$

where R_1 and R_2 are the respective radii of the contacting surfaces (+ is used where both surfaces are convex and − is used when one surface is concave) and

$$K_2 = K_G + K_M = \frac{1-\nu_G^2}{E_G} + \frac{1-\nu_M^2}{E_M}, \tag{3}$$

where E_G, ν_G, E_M and ν_M are the Young's moduli and Poisson ratios for the glass and metal surfaces [1, p.563].

Conical seats (where $R_1 = \infty$ and $K_1 = \frac{1}{2R_2}$) are commonly used where contact stresses are of concern, since these result in lower contact stresses as compared to sharp corner seats, or seats with positive secondary radius R_2. The lowest stress possible for this type of interface results when $R_1 = R_2$, and the lens surface curvature exactly matches the seat curvature. The risk when attempting to exactly match the curvatures of the lens and the seat is that it introduces the possibility of contact between the sharp edges of the spacer and the spherical lens surface if their respective radii are mismatched, or where burrs may be left at the edge of the surface by the machining process.

The compromise employed for NGS2 was to produce the seating surfaces of the spacers with a toroidal form, allowing the contacting face of the spacer to cradle the lens surface with a secondary radius of the spacer slightly greater than the radius of curvature for the lens. In this case, the form of Equation (2) becomes;

$$K_1 = \frac{R_1 - R_2}{2(R_1 R_2)}, \tag{4}$$

where the value of $R_1 - R_2$ is chosen such that the worst case machining errors (assumed to be a profile tolerance of the seats of $10\mu m$) would still provide clearance between the inner and outer edges of the seating surface of the spacers and the adjacent lens surfaces. This form is shown schematically in figure 2.

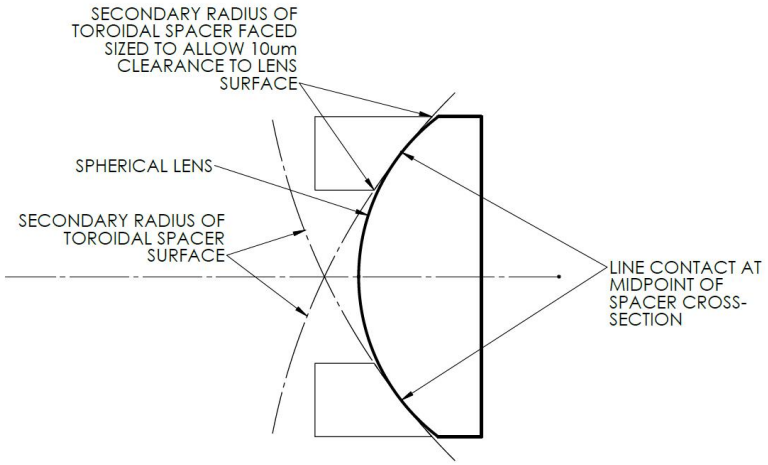

Figure 2. Schematic showing cross section of cylindrically symmetric toroidal lens seats. Note that the features are exaggerated to show the toroidal form of the seats.

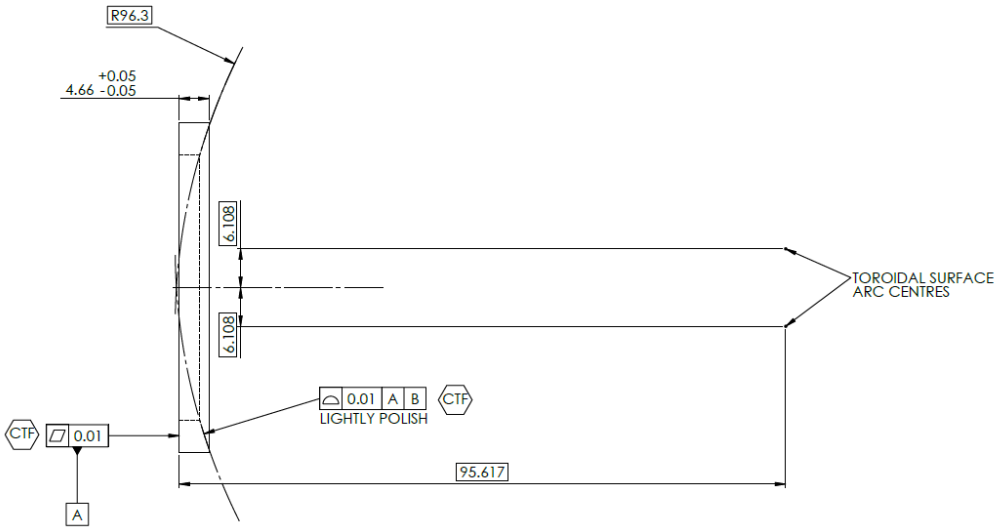

Figure 3. Example toroidal spacer mechanical tolerances.

2.2 Lens safety evaluation

The approach adopted during the design of NGS2 for evaluating the maximum stress criterion for glasses other than CaF2 was to apply the value suggested by Yoder [1, p.559] as a rule of thumb, of 6.9 MPa (1000 psi) in tension. Since all loads on the glass are applied in compression, the tension stresses are developed due to Poisson strains resulting from the compressive contact stresses. Yoder gives the magnitude of the tensile stress as compared to compressive stresses by

$$\sigma_T = \frac{\sigma_C(1-2\nu)}{3}. \tag{5}$$

2.3 CaF2 maximum stress criterion

Schwertz [2, p.12] describes the following equation and parameters for evaluating the likelihood of brittle failure of a range of optical glasses, based on applied bending stress. This approach reflects the wide distribution of failure stresses for glasses.

$$P_f = 1 - exp\left[-\left(\frac{\sigma}{\sigma_0}\right)^m\right], \tag{6}$$

where P_f = Probability of Failure, σ = applied stress, σ_0 = characteristic strength and m = Weibull modulus. For CaF2, Schwertz [2, p.13] gives the parameters $\sigma_0 = 5.0$ MPa and $m = 3.0$. This statistical approach is equally applicable to optical glasses other than CaF2, which are used in the Objective and Tube Lens Assemblies, although the calculations are not shown here since the application of the 6.9 MPa maximum stress criterion for the less delicate glasses yields a vanishingly small likelihood of failure ($>>0.01\%$).

The calculated contact stresses (in compression and tension) in the lenses at the toroidal spacer interfaces are listed in Table 1. The tension stress at each surface of the CaF2 lenses is less than 0.8 MPa. In the case of O6, the tensile stress is 3.1 MPa, although since O6 is not CaF_2, the higher stress is not a concern as it is within the 6.9 MPa criterion for less fragile glasses.

2.4 Lens spacer manufacturing validation

The design of the toroidal seats called for a strict mechanical tolerances on the toroidal face of a profile tolerance of $10\mu m$ to ensure that the spacer edges were clear of the lens, that the secondary radius of the toroidal surface

Table 1. Compressive and tension contact stresses at each of the spherical lens surfaces in the NGS2 Objective Assembly.

Lens surface	σ_C **(MPa)**	σ_T **(MPa)**	**Probability of failure (%)**
O1 - Surface 1	4.263	0.682	0.254
O1 - Surface 2	3.781	0.605	0.177
O3 - Surface 2	3.480	0.557	0.013
O4 - Surface 1	4.609	0.737	0.215
O4 - Surface 2	4.905	0.785	0.137
O5 - Surface 1	2.729	0.437	0.024
O6 - Surface 1	22.485	3.118	0.0

in the regions of contact with the lenses was predictable and consistent with the design and that unanticipated mechanical features in the spacers would not act as stress concentrators.

To test and validate the machining processes employed, the toroidal faces of each of the spacers were measured using a CMM machine. Two production methods were investigated; CNC Milling using a ball router and CNC turning, and the resulting spacers measured by the National Measurement Institute in Melbourne, Australia. The milling process was found to produce a result which was marginally outside of the required profile tolerance of $10\mu m$, whilst the CNC turning process produced a result which was well within the $10\mu m$ tolerance. The total variation from the ideal surface in the CNC produced spacers was less than $4\mu m$ (equivalent to the read limit of the CMM probe used). These results provided assurance that the spacers would not impart undue stresses to the lens in the objective and that the lenses would be correctly axially located within the Objective Housing.

2.5 Radial lens location

The wide variation of thermal expansion coefficients between the various glasses of the lenses in the objective, combined with the survival temperature range requirements for the sensor (-15 to 25 deg C) meant that the lens decentre tolerances could not be met solely by location within the common bore. The CaF2 lenses, chosen for their low dispersion characteristics, exhibit a thermal strain of 18.4 $\times 10^{-6}$/C, which is far greater than the other glasses employed in the objective. The lens materials and Coefficients of Thermal Expansion (COTE) are listed in table 2.

Table 2. Thermal expansion coefficients for the materials used in the objective assembly for NGS2.

Component	Material	COTE ($\times 10^{-6}$/C)
O1	CaF2	18.4
O2	N-KZFS4	7.3
O3	CaF2	18.4
O4	CaF2	18.4
O5	CaF2	18.4
O6	S-LAM60	5.6
Housing	304 SS	16

The common bore of the objective was made from 304 Stainless Steel, chosen for its COTE of approximately 16 $\times 10^{-6}$/C over the relevant temperature range, which was the closest available match for the COTE of CaF2.

The O2 and O6 lenses, being the only lenses made from lower thermal expansion glasses, were located in the bore by circularly symmetric, radially compliant springs, shown in Figure 4. These are shown in the assembly as the O2 and O6 centering spacers in figure 1. The spacers are formed by Electro-Discharge Machining (EDM)

which allows the production of fine internal features, without imparting residual stresses to the material. Two sets of overlapping slots form a series of thin circumferential beams, providing a radial degree of freedom for points on the inner and outer ring, whilst maintaining a high degree of stiffness for the angular alignment of the inner and outer bores. The radial degree of freedom weakly but symmetrically constrains the lens to the centre of the mounting bore, without the risk of crushing the lens as the assembly is cycled thermally.

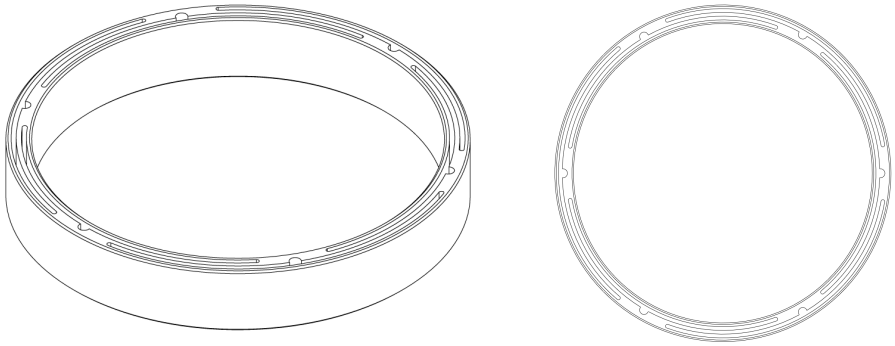

Figure 4. Radial spacer providing centring within the objective bore for O6, isometric view (left) and plan view (right).

The internal diameters for the radial spacers were sized to result in a very light interference fit with their associated lens. The spacers assembled with the lenses by heating the spacer by approximately 20 deg C before fitting over the lens. The continuous inner ring of the spacer is thin enough to absorb up the interference caused by the thermal strain mismatch between the lens and the spacer, as shown in Sec. 2.6. The outer ring of the spacer expands and contracts along with the housing, since they are made from a common material.

2.6 Compressive stress imparted by centring rings

To calculate the compressive stresses imparted to the lens by the centring spacer under the light interference fit, the section of the centring ring, inside the inner grooves can be modelled as a single ring with a thickness equal to the average of this inner section. This assumes that the parts of the spacer outside this section do not contribute to the hoop stress. Hoop stress in thin walled cylinders is given by

$$\sigma_{hoop} = \frac{Pr}{t} = \epsilon E. \tag{7}$$

where P is the internal pressure, r is the radius of the cylinder, t is the average wall thickness, ϵ is the strain in the ring and E is the elastic modulus for the ring. For a given amount of interference between the lens and spacer, ΔD, the stretching of the inner ring of the spacer gives a strain of

$$\epsilon = \frac{\Delta D}{D}. \tag{8}$$

The compressive stress is the lens is equal to the radial pressure exerted by the ring, which is obtained by solving Equation 7 for P. This stress criterion is evaluated for the MMC condition at -15 deg C, where the interference is greatest.

$$\sigma_{lens} = P = \frac{tE}{r}\frac{\Delta D}{D} \tag{9}$$

The parameters for each of the two lenses located by the centring rings are listed in Table 3 with the resulting compressive stress. For both O2 and O6, the compressive stress imparted by the centring ring is sufficiently low that it does not risk fracture of these two lenses.

Table 3. Parameters for calculation of compressive stress imparted by shrink fit of radial spacers.

Component	t (mm)	E (GPa)	r (mm)	ΔD (mm)	D (mm)	σ_{lens} (MPa)
O2	0.667	190	27.5	0.019	55.0	1.60
O6	0.667	190	20.0	0.013	40.0	2.06

2.7 Factory acceptance testing

Successful factory acceptance tests carried out at ANU in 2016 validated the lens mounting techniques employed in the objective. Performance tests of the sensor involved collection of detector images using the included calibration source for the sensor. The calibration source consists of three $15\mu m$ pinholes mounted at the focal plane of the sensor. The test images captured 94% of encircled energy within a single $16\mu m$ pixel, easily exceeding the performance specification of 80%, indicating correct alignment of all optics in the system.

Environmental survival testing was also carried out as part of the factory acceptance tests. In this test, the entire sensor was cooled to its specified survival temperature of -15 deg C at a rate of 4 deg/hour. All components in the sensor, including all optics, survived the cool down test without the overall alignment of the sensor being compromised, validating the design against the specified environmental requirement of a -15 to 25 deg C survival temperature range.

3. VELOCE OVERVIEW

Veloce is a high-resolution spectrograph, built at the Australian National University from 2016 to 2018. The first of three channels was tested and installed at the Anglo Australian Telescope in April 2018. Included in the instrument is a camera consisting of bolted plate type assembly, with lenses carried cells that are supported by the bulkheads that comprise the camera structure.

3.1 Lens cell adjustment technique

Each of the lens cells in the Veloce camera are mounted semi-kinematically to their respective bulkheads. The kinematic mounting scheme employs three equally spaced slots around the cell perimeters, that accept toleranced shafts. These shafts are mounted via closely fitting bores in the bulkheads that form the structure of the camera. A cutaway view of the camera is shown in figure 5.

The optical design of the camera called for a decentre tolerance of the entrance lens (carried by the CM1 cell as shown in figure 5) of $40\mu m$; which was the tightest decentre tolerance in the camera. This tolerance was well exceeded by the stack of mechanical tolerances under the fixed cell mounting scheme employed for the other lenses. To overcome this tolerance stack, the radial position of the CM1 cell was made adjustable by incorporating an eccentricity into the cell mounting posts. Adjustments are made by rotating the posts individually in situ using a flat head screwdriver.

The eccentricity of the posts was specified as 0.1mm, giving a total adjustment diameter of the cell axis of 0.2mm. The sensitivity of the adjustment mechanism was estimated by placing a dial gauge against the cell and making the minimum adjustments possible. It was determined through this process that repeatable motions as small as $5\mu m$ were possible via the adjustment mechanism.

4. CONCLUSIONS

The mounting techniques employed for the NGS2 Objective Barrel proved to be effective in protecting the fragile CaF2 lenses of the Objective Assembly from damage, whilst maintaining the stringent positional tolerances of the lenses. Positioning of the lenses was verified by the factory acceptance testing for NGS2, during which images from the calibration source were produced in which 94% of encircled energy was captured by a single 16um detector pixel, surpassing the specification of 80%. The radial spacers employed for the non-CaF2 lenses in the Objective Assembly ensured the centring of those lenses within their mounting bores, from first assembly throughout the testing regime.

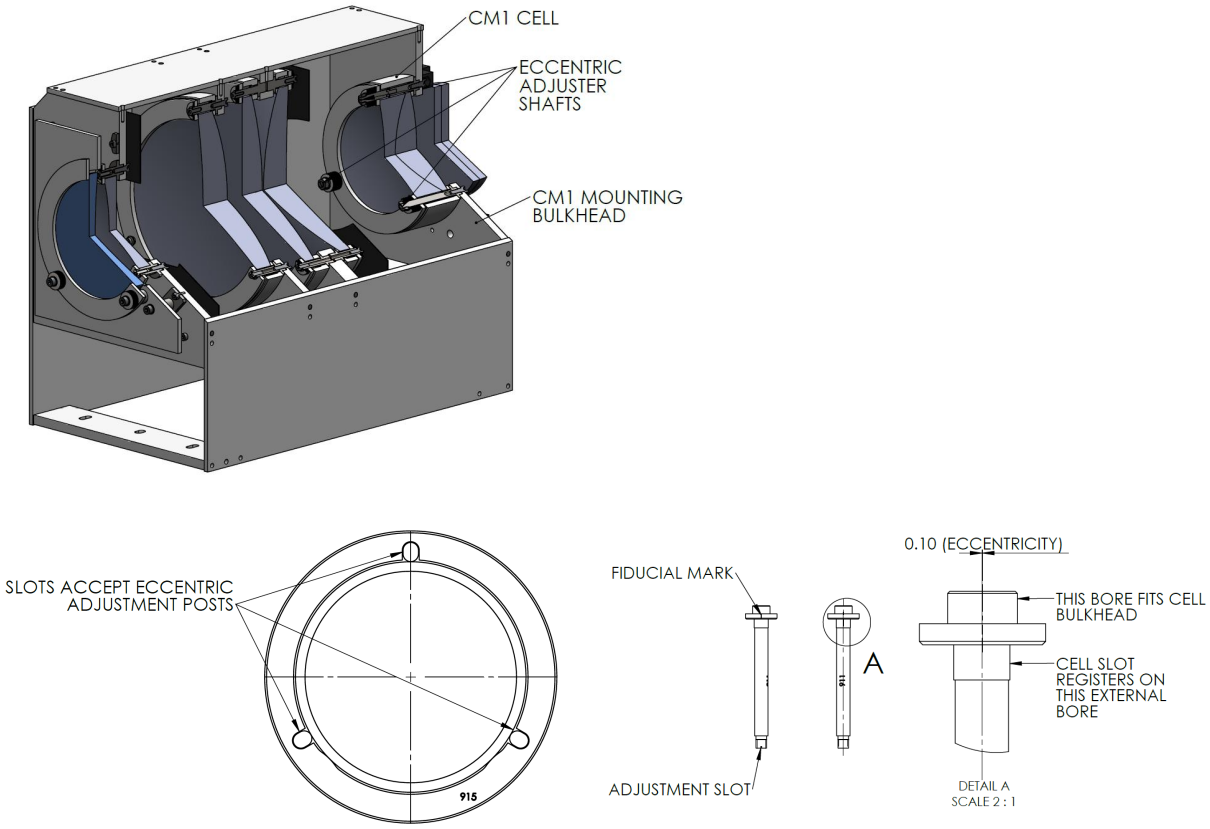

Figure 5. Cutaway view of Veloce Rosso Channel Camera assembly (top), CM1 lens cell showing slotted holes that mate with eccentric shafts (bottom left) and detail view of eccentric adjuster shafts to control position of CM1 Cell (bottom right).

The adjustment technique developed for the CM1 Cell in the Veloce Rosso Camera allowed adjustment of the decentre of the cell with a precision of approximately $5\mu m$.

REFERENCES

[1] Yoder, P. R., [*Mounting Optics in Optical Instruments*], SPIE Press, Bellingham, Washington, second ed. (2008).

[2] Schwertz, K., "Useful estimations and rules of thumb for optomechanics," (2010).